Strain localization in ductile materials: Assessment of three X-FEM-based enrichment methods

Johannes Wolf, Patrice Longère, Jean-Philippe Crété, Jean-Marc M Cadou

Mechanics Research Communications. Year	Publication Office: Elsevier UK
Editor-in-Chief: A. Rosato New Jersey Institute of Technology, Newark, New Jersey, USA Anthony.Rosato@njit.edu	

Strain localization in ductile materials: Assessment of three X-FEM-based enrichment methods

Johannes WOLF[1], Patrice LONGERE[2], Jean-Philippe CRETE[3], Jean-Marc CADOU[4]

[1]Saint-Gobain Sekurit Deutschland GmbH & Co. KG, Herzogenrath, Germany, [2]Université de Toulouse, ISAE-SUPAERO, ICA, Toulouse, France, [3]SUPMECA, Laboratoire Quartz, Saint-Ouen, France,[4]Institut de Recherche Dupuy de Lôme,CNRS UMR 6027, IRDL, Lorient, France.

*Corresponding patrice.longere@isae.fr
Tel.:+33-561.338.115
Accepted: ???????.

Abstract

The phenomenon of void coalescence induced strain localization plays an important role in the ductile failure process as the intermediate stage between diffuse damage and crack formation. The aim of the present work is double: (i) giving a framework for numerically treating the failure of ductile structures in the context of the X-FEM and (ii) assessing three different enrichment methods allowing for reproducing the intermediate stage of void coalescence induced localization within X-FEM.

Keywords: X-FEM, cohesive zone model, ductile fracture, localization.

1. Introduction

The phenomenon of void coalescence induced strain localization plays an important role in the ductile failure process, an insight which is more and more recognized in the research of failure. Accounting for strain localization requires to capture the mechanism of deformation itself and to describe its relationship with the precedent (diffuse damage) and subsequent (crack propagation) phases of failure.

There exist in the literature various ways to model the intermediate phase of strain localization. Continuum approaches attempt to describe the effects of void coalescence on the (continuum) material, see e.g. [1-2], whereas embedded-band based approaches aims at reproducing the kinematic consequences of the localization band by enriching the finite element kinematics, see e.g. [3-4].

We are here studying the capability of X-FEM, initially developed to describe crack propagation independently of the mesh topology, see [5], to reproduce strain localization. Depending on the perspective, the mechanism of strain localization can be described via strong, weak or regularized discontinuity approach.

In the strong discontinuity method (SDM), the complex micro-mechanisms which take place during strain localization can be assumed to be collapsed into a surface which corresponds to the experimental observation of the presence of a meso-crack. In contrast to the macro-crack which is also represented by a strong discontinuity, the meso-crack is not continuous along its propagation path as it may be interrupted by zones of material cohesion and it can thus be assumed to still carry stresses. In a similar context, e.g. when it is about to describe the progressive transition from damage to fracture, there are the works of [6-8]. In the weak discontinuity method (WDM), strain localization is shown to go along with void coalescence which occurs in a narrow zone. This band of physically non-zero width accommodates large portions of damage and plastic deformation. Examples from the literature are the works in [3-4,9]. Regarding the regularized discontinuity method (RDM), it is assumed that strain localization cannot appear in a

sharply confined band. Then, the strain field across the band is rather viewed in a continuous (smooth) manner. Thus, the localized strain is distributed in a thin zone and the maximal strain is found in the very center of the band. A similar approach can be found in certain models of shear banding. Examples from the literature are the works in [10-11].

The aim of the present work is double: (i) giving a framework for numerically treating the failure of ductile structures in the context of the X-FEM and (ii) assessing three different enrichment methods allowing for reproducing the intermediate stage of void coalescence induced localization. For this purpose, the different kinematic fields are discussed and the principle of virtual work is stated which the three methods are derived from. Moreover, the enrichment technique which is used for each method is specified.

In Section 2 is recalled the principle of the standard X-FEM. The three considered methods are detailed in Section 3 and concluding remarks are given in Section 4.

2. Standard X-FEM

In the standard X-FEM framework, see [1], the continuous displacement field $\hat{\mathbf{u}}(\mathbf{x})$ of a given finite element containing any part of the strong discontinuity is assumed to be enriched by a discontinuous field $\breve{\mathbf{u}}_D(\mathbf{x})$ which is supposed to represent the kinematics of the discontinuity and a singular field $\breve{\mathbf{u}}_S(\mathbf{x})$ which is supposed to represent the singularity near the crack tip. In the case of a strongly non-linear elasto-plastic ductile material, the singular terms in the enhanced displacement formulation can be neglected (see [12]), i.e. $\breve{\mathbf{u}}_S(\mathbf{x})=\mathbf{0}$. The superposition of the continuous and discontinuous fields yields the total displacement field $\mathbf{u}(\mathbf{x})$ of the form

$$\begin{aligned}\mathbf{u}(\mathbf{x}) &= \hat{\mathbf{u}}(\mathbf{x})+\breve{\mathbf{u}}_D(\mathbf{x}) \\ &= \hat{\mathbf{u}}(\mathbf{x})+H(s)\tilde{\mathbf{u}}(\mathbf{x})\end{aligned} \tag{1}$$

where the function $H(s)$ is the modified Heaviside function $H(s)=\begin{cases}+1 & s\geq 0\\ -1 & s<0\end{cases}$; s is the signed distance function with respect to the center line of the strong discontinuity, see Fig.1.

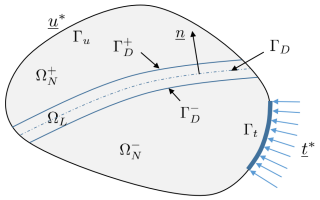

Figure 1: Body crossed by a localization band

The sign of the distance function is determined in accordance with the orientation of the normal vector $\mathbf{n}$ of the localization band. The symmetric part of the gradient of $\mathbf{u}(\mathbf{x})$ in (1) accordingly is

$$\begin{aligned}\nabla^s\mathbf{u}(\mathbf{x}) &= \nabla^s\hat{\mathbf{u}}(\mathbf{x})+H(s)\nabla^s\tilde{\mathbf{u}}(\mathbf{x}) \\ &\quad +\left[\tilde{\mathbf{u}}(\mathbf{x})\otimes\nabla H(s)\right]^s\end{aligned} \tag{2}$$

Using $\nabla H(s)=\dfrac{\partial H}{\partial s}\nabla s=\gamma(s)\mathbf{n}$ where γ denotes the Dirac's delta distribution, (2) becomes

$$\begin{aligned}\nabla^s\mathbf{u}(\mathbf{x}) &= \nabla^s\hat{\mathbf{u}}(\mathbf{x})+H(s)\nabla^s\tilde{\mathbf{u}}(\mathbf{x}) \\ &\quad +\gamma(s)\left[\tilde{\mathbf{u}}(\mathbf{x})\otimes\mathbf{n}\right]^s\end{aligned} \tag{3}$$

The bulk strain is defined as follows

$$\boldsymbol{\varepsilon}_{bulk}(\mathbf{u}(\mathbf{x}))=\nabla^s\hat{\mathbf{u}}(\mathbf{x})+H(s)\nabla^s\tilde{\mathbf{u}}(\mathbf{x}) \tag{4}$$

Introducing any admissible virtual variation of displacements $\delta\mathbf{u}$ and applying the divergence theorem yield the principle of virtual work as

$$\int_\Omega \delta\boldsymbol{\varepsilon}_{bulk}(\delta\mathbf{u}):\boldsymbol{\sigma}_{bulk}(\mathbf{u})\,d\Omega=\int_{\Gamma_t}\delta\hat{\mathbf{u}}\cdot\mathbf{t}^*\,d\Gamma \tag{5}$$

where $\boldsymbol{\sigma}_{bulk}$ and $\mathbf{t}^*$ stand for the stress and the external surface forces respectively (neglecting inertia and body forces). The use of the Bubnov-Galerkin approach, i.e. the test functions are chosen from the same space as the trial functions, see (1), yields

$$\delta\mathbf{u}=\delta\hat{\mathbf{u}}+H(s)\delta\tilde{\mathbf{u}} \tag{6}$$

The discrete displacement and strain fields of a given finite element containing any part of the strong discontinuity and their variations are interpolated as follows (using matrix notation from now on)

$$\begin{aligned}&\hat{\mathbf{u}}=\mathbf{N}\mathbf{a};\tilde{\mathbf{u}}=\mathbf{N}\mathbf{b};\nabla^s\hat{\mathbf{u}}=\mathbf{B}\mathbf{a}\ ;\ \nabla^s\tilde{\mathbf{u}}=\mathbf{B}\mathbf{b}\\ &\delta\hat{\mathbf{u}}=\mathbf{N}\delta\mathbf{a};\delta\tilde{\mathbf{u}}=\mathbf{N}\delta\mathbf{b}\ ;\ \nabla^s\delta\hat{\mathbf{u}}=\mathbf{B}\delta\mathbf{a}\ ;\ \nabla^s\delta\tilde{\mathbf{u}}=\mathbf{B}\delta\mathbf{b}\end{aligned} \tag{7}$$

where $\mathbf{a}$ and $\mathbf{b}$ are the nodal and additional degrees of freedom (dof). The $\mathbf{B}$-matrix in (7) contains the spatial derivatives of the interpolation functions $\mathbf{N}$, so that

$$\mathbf{u}=\mathbf{N}\mathbf{a}+H(s)\mathbf{N}\mathbf{b}\ ;\ \delta\mathbf{u}=\mathbf{N}\delta\mathbf{a}+H(s)\mathbf{N}\delta\mathbf{b} \tag{8}$$

and

$$\begin{aligned}\boldsymbol{\varepsilon}_{bulk}(\mathbf{u}) &= \mathbf{B}\mathbf{a}+H(s)\mathbf{B}\mathbf{b}\\ \delta\boldsymbol{\varepsilon}_{bulk}(\mathbf{u}) &= \mathbf{B}\delta\mathbf{a}+H(s)\mathbf{B}\delta\mathbf{b}\end{aligned} \tag{9}$$

Injecting (9) into (5) yields

$$\int_\Omega\left(\mathbf{B}\delta\mathbf{a}+H\mathbf{B}\delta\mathbf{b}\right)\boldsymbol{\sigma}_{bulk}(\mathbf{u})\,d\Omega=\int_{\Gamma_t}\mathbf{N}\delta\mathbf{a}\,\mathbf{t}^*\,d\Gamma \tag{10}$$

As $\delta\mathbf{a}$ and $\delta\mathbf{b}$ in (10) are independent, the use of the discretized variations of the displacements and strains in (5) allows for obtaining two separate weak equilibrium equations:

$$\begin{aligned}&\int_\Omega\mathbf{B}^T\boldsymbol{\sigma}_{bulk}(\mathbf{u})\,d\Omega=\int_{\Gamma_t}\mathbf{N}^T\mathbf{t}^*\,d\Gamma\\ &\int_\Omega H\mathbf{B}^T\boldsymbol{\sigma}_{bulk}(\mathbf{u})\,d\Omega=0\end{aligned} \tag{11}$$

To determine the state of equilibrium involving a non-linear material behavior, an incremental-iterative solution procedure is used. Therefore, the

stress-strain relationship has to be brought into a rate form. The bulk stress rate is computed using the continuum tangent modulus $\mathbf{L}_{bulk}$ as follows

$$\dot{\boldsymbol{\sigma}}_{bulk} = \mathbf{L}_{bulk}\dot{\boldsymbol{\varepsilon}}_{bulk} = \mathbf{L}_{bulk}\left(\mathbf{B}\dot{\mathbf{a}} + H\mathbf{B}\dot{\mathbf{b}}\right) \tag{12}$$

The set of discrete linearized equations involving the incremental displacements $d\mathbf{a}$ and $d\mathbf{b}$ between steps n and $n+1$ finally gives

$$\begin{bmatrix}\mathbf{K}_{aa} & \mathbf{K}_{ab}\\ \mathbf{K}_{ba} & \mathbf{K}_{bb}\end{bmatrix}\begin{Bmatrix}d\mathbf{a}\\ d\mathbf{b}\end{Bmatrix}_{n+1} = \begin{Bmatrix}\mathbf{f}_a^{ext}\\ \mathbf{f}_b^{ext}\end{Bmatrix}_{n+1} - \begin{Bmatrix}\mathbf{f}_a^{int}\\ \mathbf{f}_b^{int}\end{Bmatrix}_{n} \tag{13}$$

where the components of the stiffness matrix are computed as follows

$$\begin{aligned}&\mathbf{K}_{aa} = \int_\Omega \mathbf{B}^T\mathbf{L}_{bulk}\mathbf{B}d\Omega \;;\; \mathbf{K}_{bb} = \int_\Omega \mathbf{B}^T\mathbf{L}_{bulk}\mathbf{B}d\Omega\\ &\mathbf{K}_{ab} = \int_\Omega H\mathbf{B}^T\mathbf{L}_{bulk}\mathbf{B}d\Omega = \mathbf{K}_{ba}\end{aligned} \tag{14}$$

and the internal and external force vectors are calculated from

$$\begin{aligned}&\mathbf{f}_a^{ext} = \int_{\Gamma_t}\mathbf{N}^T\mathbf{t}^* d\Gamma \;\;;\;\; \mathbf{f}_b^{ext} = 0\\ &\mathbf{f}_a^{int} = \int_\Omega \mathbf{B}^T\boldsymbol{\sigma}_{bulk}d\Omega;\; \mathbf{f}_b^{int} = \int_\Omega H\mathbf{B}^T\boldsymbol{\sigma}_{bulk}d\Omega\end{aligned} \tag{15}$$

3. Enlarged X-FEM based methods under consideration

It should be noted that by definition a strong discontinuity involves a discontinuity of the displacement/velocity field, as for a crack, whereas a weak discontinuity involves a discontinuity of the gradient of the displacement/velocity field, as for a localization band. In the enlarged X-FEM framework considered herein, the total displacement field $\mathbf{u}(\mathbf{x})$ can be written in the form

$$\mathbf{u}(\mathbf{x}) = \hat{\mathbf{u}}(\mathbf{x}) + H_w(s)\tilde{\mathbf{u}}(\mathbf{x}) \tag{16}$$

where the function $H_w(s)$ is an adapted version of the modified Heaviside function in (1). Based on the enriched displacement field (16), the strain field is computed as follows

$$\begin{aligned}\boldsymbol{\varepsilon}(\mathbf{u}(\mathbf{x})) = \nabla^s\mathbf{u}(\mathbf{x}) &= \nabla^s\hat{\mathbf{u}}(\mathbf{x}) + H_w(s)\nabla^s\tilde{\mathbf{u}}(\mathbf{x})\\ &+ \gamma_w(s)\left[\tilde{\mathbf{u}}(\mathbf{x})\otimes\mathbf{n}\right]^s\end{aligned} \tag{17}$$

where

$$\gamma_w(s) = \frac{\partial H_w(s)}{\partial s} \tag{18}$$

denotes an adapted version of the classical Dirac's delta distribution.

We are now defining

$$\begin{aligned}&\boldsymbol{\varepsilon}_{cont}(\mathbf{x}) = \nabla^s\hat{\mathbf{u}}(\mathbf{x}) \;;\; \boldsymbol{\varepsilon}_{loc}(\mathbf{x}) = \gamma_w(s)\left[\tilde{\mathbf{u}}(\mathbf{x})\otimes\mathbf{n}\right]^s\\ &\boldsymbol{\varepsilon}_{bulk}(\mathbf{x}) = \nabla^s\hat{\mathbf{u}}(\mathbf{x}) + H_w(s)\nabla^s\tilde{\mathbf{u}}(\mathbf{x})\\ &\boldsymbol{\varepsilon}_{band}(\mathbf{x}) = \nabla^s\hat{\mathbf{u}}(\mathbf{x}) + \gamma_w(s)\left[\tilde{\mathbf{u}}(\mathbf{x})\otimes\mathbf{n}\right]^s\\ &\qquad = \boldsymbol{\varepsilon}_{cont}(\mathbf{x}) + \boldsymbol{\varepsilon}_{loc}(\mathbf{x})\end{aligned} \tag{19}$$

where $\boldsymbol{\varepsilon}_{cont}(\mathbf{x})$ denotes the continuous strain which prevails *before* the onset of localization; $\boldsymbol{\varepsilon}_{bulk}(\mathbf{x})$ the bulk strain *in presence of* the localization band; $\boldsymbol{\varepsilon}_{loc}(\mathbf{x})$ the localization-induced overstrain which includes contributions normal and tangential to the band and $\boldsymbol{\varepsilon}_{band}(\mathbf{x})$ the strain in the band. The discrete displacement and strain fields of a given finite element containing any part of the band and their variations are interpolated as follows

$$\mathbf{u} = \mathbf{N}\mathbf{a} + H_w\mathbf{N}\mathbf{b} \tag{20}$$

and

$$\boldsymbol{\varepsilon} = \mathbf{B}\mathbf{a} + H_w\mathbf{B}\mathbf{b} + (\gamma_w\mathbf{n})\mathbf{N}\mathbf{b} \tag{21}$$

yielding

$$\begin{aligned}&\boldsymbol{\varepsilon}_{cont} = \mathbf{B}\mathbf{a} \;\;;\;\; \boldsymbol{\varepsilon}_{bulk} = \mathbf{B}\mathbf{a} + H_w\mathbf{B}\mathbf{b}\\ &\boldsymbol{\varepsilon}_{loc} = (\gamma_w\mathbf{n})\mathbf{N}\mathbf{b} \;\;;\;\; \boldsymbol{\varepsilon}_{band} = \mathbf{B}\mathbf{a} + (\gamma_w\mathbf{n})\mathbf{N}\mathbf{b}\end{aligned} \tag{22}$$

The advantage of using the discontinuous enrichment formulation is that any arbitrary profile of the displacement field across the band can be prescribed. Depending on the different viewpoints (discussed below), the displacement field may be described by a strong, weakly or (non-linearly) regularized discontinuity. It should be noted that the weak discontinuity is a special type of regularization of the strong discontinuity. Yet, in this work the class of 'weak discontinuity' is regarded as being different from the class of 'regularized discontinuity' which is referred to as non-linearly distributed (continuous) profile.

Three different viewpoints of the localization band are to be studied successively. As a means of comparison, an appropriate discretization framework is elaborated, computational issues are discussed and capabilities for describing the transition from continuum mechanics and the transition to fracture mechanics are assessed.

.

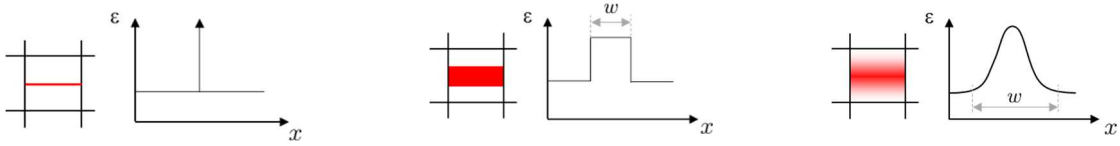

a) 'cohesive' strong discontinuity b) weak discontinuity c) regularized discontinuity.

Figure 2: Strain profiles. The length scale *w* is related to the localization bandwidth

3.1. Strong discontinuity method (SDM)

In this context, i.e. cohesive strong discontinuity, function $H_w(s)$ corresponds to the modified Heaviside function as in (1) and $\gamma_w(s)$ equals to (18). The strain profile can then be

depicted as in Fig.2a. The virtual internal work can be written

$$\int_\Omega \delta\boldsymbol{\varepsilon}(\delta\mathbf{u})\boldsymbol{\sigma}(\mathbf{u})d\Omega = \int_{\Gamma_t} \delta\mathbf{u}\cdot\mathbf{t}^* d\Gamma \tag{23}$$

Injecting (20), (21) and (22) into (23) yields

$$\begin{aligned}&\int_\Omega (\mathbf{B}\delta\mathbf{a} + H_w\mathbf{B}\delta\mathbf{b})\cdot\boldsymbol{\sigma}_{bulk}(\mathbf{u})d\Omega \\ &\quad + \int_\Omega (\gamma_w\mathbf{n})\mathbf{N}\delta\mathbf{b}\cdot\boldsymbol{\sigma}_{loc}(\mathbf{u})d\Omega \\ &\quad = \int_{\Gamma_t}\mathbf{N}\delta\mathbf{a}\cdot\mathbf{t}^* d\Gamma + \int_{\Gamma_t} H_w\mathbf{N}\delta\mathbf{b}\cdot\mathbf{t}^* d\Gamma\end{aligned} \tag{24}$$

Noting that

$$\int_\Omega (\gamma_w\mathbf{n})\mathbf{N}\delta\mathbf{b}\cdot\boldsymbol{\sigma}_{loc}(\mathbf{u})d\Omega = 2\int_{\Gamma_D}\mathbf{N}\delta\mathbf{b}\cdot\mathbf{T}_{loc}d\Gamma \tag{25}$$

the system of equations (24) then yields

$$\begin{aligned}&\int_\Omega \mathbf{B}^T\boldsymbol{\sigma}_{bulk}(\mathbf{u})d\Omega = \int_{\Gamma_t}\mathbf{N}^T\mathbf{t}^* d\Gamma \\ &\int_\Omega H_w\mathbf{B}^T\boldsymbol{\sigma}_{bulk}(\mathbf{u})d\Omega + 2\int_{\Gamma_D}\mathbf{N}^T\mathbf{T}_{loc}(\mathbf{u})d\Gamma = \\ &\qquad \int_{\Gamma_t} H_w\mathbf{N}^T\mathbf{t}^* d\Gamma\end{aligned} \tag{26}$$

Where $\mathbf{T}_{loc}$ is the (cohesive) traction force. The first equation constitutes the equilibrium in the continuous field (bulk material). The second equation describes the traction continuity across the discontinuity in a weak sense, where continuity is established between the integral over the entire continuous domain Ω_N, i.e. $\Omega_N^+ \cup \Omega_N^-$, see Fig.1, and the integral over the cohesive surface, which is typical for the KOS formulation according to the terminology in [13]. So the traction continuity appears as a result of the consequent application of the principle of virtual work and is not imposed as an additional equation. This is in contrast to the SOS [3-4] and SKON [9,14] formulations (see [13]) in the context of the E-FEM, where the traction continuity condition is explicitly imposed at the interface and thus allows for a more accurate stress computation. The bulk stress rate is computed according to (12). In the same way, the traction rate of the cohesive law in (25-26) reads

$$\dot{\mathbf{T}}_{loc} = \mathbf{D}_{loc}[\![\dot{\mathbf{u}}]\!] \;;\; [\![\dot{\mathbf{u}}]\!] = 2\mathbf{N}\dot{\mathbf{b}} \tag{27}$$

where $\mathbf{D}_{loc}$ is the cohesive tangent modulus and $[\![\dot{\mathbf{u}}]\!]$ the displacement jump rate of the crack lips. The components of the stiffness matrix in (13) coming from (26-27) are computed as follows

$$\begin{aligned}\mathbf{K}_{aa} &= \int_\Omega \mathbf{B}^T\mathbf{L}_{bulk}\mathbf{B}\,d\Omega \\ \mathbf{K}_{ab} &= \int_\Omega H_w\mathbf{B}^T\mathbf{L}_{bulk}\mathbf{B}\,d\Omega = \mathbf{K}_{ba} \\ \mathbf{K}_{bb} &= \int_\Omega \mathbf{B}^T\mathbf{L}_{bulk}\mathbf{B}\,d\Omega + 4\int_{\Gamma_o}\mathbf{N}^T\mathbf{D}_{loc}\mathbf{N}\,d\Gamma\end{aligned} \tag{28}$$

and the internal and external force vectors are calculated from

$$\begin{aligned}&\mathbf{f}_a^{ext} = \int_{\Gamma_t}\mathbf{N}^T\mathbf{t}^* d\Gamma \;;\; \mathbf{f}_b^{ext} = \int_{\Gamma_t} H_w\mathbf{N}^T\mathbf{t}^* d\Gamma \\ &\mathbf{f}_a^{int} = \int_\Omega \mathbf{B}^T\boldsymbol{\sigma}_{bulk}d\Omega \\ &\mathbf{f}_b^{int} = \int_\Omega H_w\mathbf{B}^T\boldsymbol{\sigma}_{bulk}d\Omega + 2\int_{\Gamma_D}\mathbf{N}^T\mathbf{T}_{loc}d\Gamma\end{aligned} \tag{29}$$

The incorporation of a discontinuity into the element using X-FEM requires the application of special integration techniques to evaluate the integrals at the Gauss points in the continuum bulk. The widely used subtriangulation method of [5] is not adapted to ductile materials for which the history- and path-dependent variables need to be tracked. Thus it is rather advantageous to use the approach of [12] where the two-dimensional (2D) element is subdivided into 16 rectangles which are each integrated by the 4-points Gauss rule (64 Gauss points in total), see Fig.3.

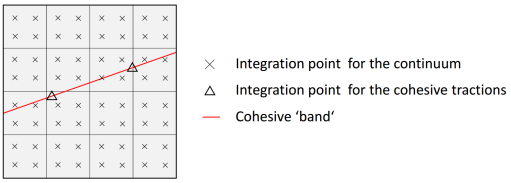

Figure 3: Integration scheme for a 2D quadrilateral element cut by a cohesive 'band'

The contributions of the cohesive tractions to the elemental equations, that is the line integrals along Γ_D in $\mathbf{K}_{bb}$ and $\mathbf{f}_b^{int}$, can be evaluated by using two additional (standard) Gauss points (GP) (see e.g. [15]) or just one GP to reduce the calculation time. The GPs are positioned along the one-dimensional (1D) cohesive segment within the localized element, see Fig.3. The SDM as described above has been implemented in the engineering FE code Abaqus by [16].

3.2. Weak discontinuity method (WDM)

In the WDM, functions $H_w(s)$ and $\gamma_w(s)$ in (17) are reported in Table 1 where the localization bandwidth related length scale w depends on the material and loading conditions. The corresponding strain profile is depicted in Fig.2b.

Table 1: Functions $H_w(s)$ and $\gamma_w(s)$ for a weak discontinuity.

	$s < -\frac{w}{2}$	$-\frac{w}{2} \le s < +\frac{w}{2}$	$s \ge +\frac{w}{2}$
$H_w(s)$	-1	$\frac{2}{w}s$	$+1$
$\gamma_w(s)$	0	$\frac{2}{w}$	0

In the case of a weak discontinuity, the left side of the virtual internal work (23) can be rewritten as follows

$$\begin{aligned}&\int_\Omega \delta\boldsymbol{\varepsilon}(\delta\mathbf{u}):\boldsymbol{\sigma}(\mathbf{u})d\Omega = \int_{\Omega_N}\delta\boldsymbol{\varepsilon}_{bulk}(\delta\mathbf{u}):\boldsymbol{\sigma}_{bulk}(\mathbf{u})d\Omega \\ &+\int_{\Omega_L}\delta\boldsymbol{\varepsilon}_{band}(\delta\mathbf{u}):\boldsymbol{\sigma}_{band}(\mathbf{u})d\Omega\end{aligned} \tag{30}$$

where

$$\int_{\Omega_L}\therefore d\Omega = \int_{-w/2}^{+w/2}\int_{\Gamma_D}\therefore dnd\Gamma = w\int_{\Gamma_D}\therefore d\Gamma \tag{31}$$

yielding the following weak form of the equilibrium equations

$$\int_{\Omega_N} \delta\boldsymbol{\varepsilon}_{bulk}(\delta\mathbf{u})\boldsymbol{\sigma}_{bulk}(\mathbf{u})d\Omega + w\int_{\Gamma_D} \delta\boldsymbol{\varepsilon}_{band}(\delta\mathbf{u})\boldsymbol{\sigma}_{band}(\mathbf{u})d\Gamma = \int_{\Gamma_t} \delta\hat{\mathbf{u}}\cdot\mathbf{t}^* d\Gamma + \int_{\Gamma_t} H_w\delta\tilde{\mathbf{u}}\cdot\mathbf{t}^* d\Gamma \quad (32)$$

Injecting (22) (except for the localization part of the strain and the continuous strain) into (32) leads to

$$\int_{\Omega_N} (\mathbf{B}\delta\mathbf{a} + H_w\mathbf{B}\delta\mathbf{b})\boldsymbol{\sigma}_{bulk}(\mathbf{u})d\Omega + w\int_{\Gamma_D} (\mathbf{B}\delta\mathbf{a} + (\gamma_w\mathbf{n})\mathbf{N}\delta\mathbf{b})\boldsymbol{\sigma}_{band}(\mathbf{u})d\Gamma = \int_{\Gamma_t} \mathbf{N}\delta\mathbf{a}\cdot\mathbf{t}^* d\Gamma + \int_{\Gamma_t} H_w\mathbf{N}\delta\mathbf{b}\cdot\mathbf{t}^* d\Gamma \quad (33)$$

Finally, the system of equations reads

$$\begin{aligned} &\int_{\Omega_N} \mathbf{B}^T\boldsymbol{\sigma}_{bulk}(\mathbf{u})d\Omega + w\int_{\Gamma_D} \mathbf{B}^T\boldsymbol{\sigma}_{band}(\mathbf{u})d\Gamma = \int_{\Gamma_t} \mathbf{N}^T\mathbf{t}^* d\Gamma \\ &\int_{\Omega_N} H_w\mathbf{B}^T\boldsymbol{\sigma}_{bulk}(\mathbf{u})d\Omega + 2\int_{\Gamma_D} \mathbf{N}^T(\boldsymbol{\sigma}_{band}(\mathbf{u}).\mathbf{n})d\Gamma = \int_{\Gamma_t} H_w\mathbf{N}^T\mathbf{t}^* d\Gamma \end{aligned} \quad (34)$$

When comparing (34) for WDM with (26) for SDM, two observations can be made: (i) in the first equation of (34), a second surface integral appears which results from the band continuum, and (ii) the second equation has the same appearance, but now the tractions are evaluated from the continuum stress in the band. The stress rates outside is computed as for (12) and inside the band as follow

$$\dot{\boldsymbol{\sigma}}_{band} = \mathbf{L}_{band}\dot{\boldsymbol{\varepsilon}}_{band} = \mathbf{L}_{band}(\mathbf{B}\dot{\mathbf{a}} + (\gamma_w\mathbf{n})\mathbf{N}\dot{\mathbf{b}}) \quad (35)$$

with possibly $\mathbf{L}_{bulk} = \mathbf{L}_{band} = \mathbf{L}$.

The components of the stiffness matrix in (13-14) coming from (34-35) are computed as follows

$$\begin{aligned} \mathbf{K}_{aa} &= \int_{\Omega_N} \mathbf{B}^T\mathbf{L}_{bulk}\mathbf{B}d\Omega + w\int_{\Gamma_D} \mathbf{B}^T\mathbf{L}_{band}\mathbf{B}d\Gamma \\ \mathbf{K}_{ab} &= \int_{\Omega_N} H_w\mathbf{B}^T\mathbf{L}_{bulk}\mathbf{B}d\Omega + 2\int_{\Gamma_D} \mathbf{B}^T\mathbf{L}_{band}\overline{\mathbf{N}}d\Gamma \\ \mathbf{K}_{ba} &= \mathbf{K}^T{}_{ab} \\ \mathbf{K}_{bb} &= \int_{\Omega_N} \mathbf{B}^T\mathbf{L}_{bulk}\mathbf{B}d\Omega + 2\int_{\Gamma_D} \gamma_w\overline{\mathbf{N}}^T\mathbf{L}_{band}\overline{\mathbf{N}}d\Gamma \end{aligned} \quad (36)$$

and the internal and external force vectors are calculated from

$$\begin{aligned} \mathbf{f}_a^{ext} &= \int_{\Gamma_t} \mathbf{N}^T\mathbf{t}^* d\Gamma \;\; ; \;\; \mathbf{f}_b^{ext} = \int_{\Gamma_t} H_w\mathbf{N}^T\mathbf{t}^* d\Gamma \\ \mathbf{f}_a^{int} &= \int_{\Omega_N} \mathbf{B}^T\boldsymbol{\sigma}_{bulk}d\Omega + w\int_{\Gamma_D} \mathbf{B}^T\boldsymbol{\sigma}_{band}d\Gamma \\ \mathbf{f}_b^{int} &= \int_{\Omega_N} H_w\mathbf{B}^T\boldsymbol{\sigma}_{bulk}d\Omega + 2\int_{\Gamma_D} \mathbf{N}^T(\boldsymbol{\sigma}_{band}.\mathbf{n})d\Gamma \end{aligned} \quad (37)$$

with $\overline{\mathbf{N}} = (\mathbf{N}\otimes\mathbf{n})^s$.

The integration of the continuous terms can be achieved in the same way as described previously in subsection 3.1, i.e. by using 64 fixed integration points. The integration of the terms concerning the localized band requires some additional reflections. Regarding the simplification made in (25), the integral over the localization band Ω_L could be transformed into a surface integral over Γ_D by still maintaining the continuous character of the localized material. This step allows for applying 1D-integration with two GPs along Γ_D, see Fig.4, to reduce computation time, and prevents from using any non-standard 2D-integration scheme adapted to the oriented localization band in the element.

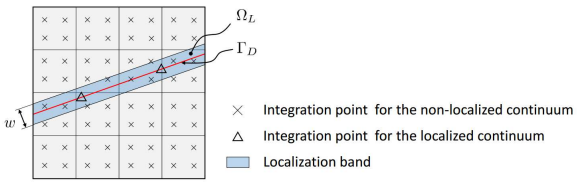

Figure 4: Integration scheme for a 2D quadrilateral element cut by a cohesive 'band'.

3.3. Regularized discontinuity method (RDM)

An example for the functions $H_w(s)$ and $\gamma_w(s)$ for RDM is given in Table 2.

Table 2: Example for functions $H_w(s)$ and $\gamma_w(s)$ for a regularized discontinuity.

	$s < -\frac{w}{2}$	$-\frac{w}{2} \le s < +\frac{w}{2}$	$s \ge +\frac{w}{2}$
$H_w(s)$	–1	$\tanh\left(\frac{4}{w}s\right)$	+1
$\gamma_w(s)$	0	$\frac{4}{w}\left[1-\tanh^2\left(\frac{4}{w}s\right)\right]$	0

The corresponding strain profile is depicted in Fig.2c.

In the RDM, the simplification deduced from (31) for WDM no longer applies due to the non-linearity (inhomogeneity) of the stress and strain field across the band. In this context, hypotheses have been notably proposed in [11] consisting in assuming that the bulk strain and localized strain (which are components of the total strain, see the decomposition employed in (17) and below), and their conjugate stress fields, are uncoupled mechanisms from the mechanical viewpoint. However, this hypothesis has been made by pure mathematical motivations, and the relation to physics remains questionable. Furthermore, it is proposed in the context of elasto-damaging materials, but no analysis has been made so far for ductile materials. The principle of virtual work reads

$$\int_{\Omega_N} \boldsymbol{\varepsilon}(\delta\mathbf{u})\boldsymbol{\sigma}(\mathbf{u})d\Omega + \int_{\Omega_L} \boldsymbol{\varepsilon}(\delta\mathbf{u})\boldsymbol{\sigma}(\mathbf{u})d\Omega = \int_{\Gamma_t} \delta\hat{\mathbf{u}}\cdot\mathbf{t}^* d\Gamma + \int_{\Gamma_t} H_w\delta\tilde{\mathbf{u}}\cdot\mathbf{t}^* d\Gamma \quad (38)$$

Injecting (21) into (38) leads to

$$\int_{\Omega_N} (\mathbf{B}\delta\mathbf{a} + H_w\mathbf{B}\delta\mathbf{b})\boldsymbol{\sigma}(\mathbf{u})d\Omega + \int_{\Omega_L} (\mathbf{B}\delta\mathbf{a} + (H_w\mathbf{B} + (\gamma_w\mathbf{n})\mathbf{N})\delta\mathbf{b})\boldsymbol{\sigma}(\mathbf{u})d\Omega = \int_{\Gamma_t} \mathbf{N}\delta\mathbf{a}\cdot\mathbf{t}^* d\Gamma + \int_{\Gamma_t} H_w\mathbf{N}\delta\mathbf{b}\cdot\mathbf{t}^* d\Gamma \quad (39)$$

Hence

$$\int_{\Omega_N}\mathbf{B}^T\boldsymbol{\sigma}\,d\Omega+\int_{\Omega_L}\mathbf{B}^T\boldsymbol{\sigma}\,d\Omega=\int_{\Gamma_t}\mathbf{N}^T\mathbf{t}^*\,d\Gamma$$
$$\int_{\Omega_N}H_w\mathbf{B}^T\boldsymbol{\sigma}\,d\Omega+\int_{\Omega_L}H_w\mathbf{B}^T\boldsymbol{\sigma}\,d\Omega+\int_{\Omega_L}\gamma_w\overline{N}^T\boldsymbol{\sigma}\,d\Omega \qquad (40)$$
$$=\int_{\Gamma_t}H_w\mathbf{N}^T\mathbf{t}^*\,d\Gamma$$

The stress rates is computed as follow

$$\dot{\boldsymbol{\sigma}}=\mathbf{L}\dot{\boldsymbol{\varepsilon}}=\mathbf{L}\left(\mathbf{B}\dot{\mathbf{a}}+H_w\mathbf{B}\dot{\mathbf{b}}+\left(\gamma_w\mathbf{n}\right)\mathbf{N}\dot{\mathbf{b}}\right) \qquad (41)$$

The components of the stiffness matrix in (13) coming from (40) and (41) are computed as follows

$$\mathbf{K}_{aa}=\int_{\Omega_N}\mathbf{B}^T\mathbf{L}\mathbf{B}d\Omega+\int_{\Omega_L}\mathbf{B}^T\mathbf{L}\mathbf{B}d\Omega$$
$$\mathbf{K}_{ab}=\int_{\Omega_N}H_w\mathbf{B}^T\mathbf{L}\mathbf{B}d\Omega+\int_{\Omega_L}H_w\mathbf{B}^T\mathbf{L}\mathbf{B}d\Omega+\int_{\Omega_L}\gamma_w\mathbf{B}^T\mathbf{L}\overline{\mathbf{N}}d\Omega$$
$$\mathbf{K}_{ba}=\mathbf{K}^T{}_{ab} \qquad (42)$$
$$\mathbf{K}_{bb}=\int_{\Omega_N}\mathbf{B}^T\mathbf{L}\mathbf{B}d\Omega+\int_{\Omega_L}H_w^2\mathbf{B}^T\mathbf{L}\mathbf{B}d\Omega+\int_{\Omega_L}H_w\gamma_w\mathbf{B}^T\mathbf{L}\overline{\mathbf{N}}d\Omega+$$
$$\int_{\Omega_L}\gamma_wH_w\overline{\mathbf{N}}^T\mathbf{L}\mathbf{B}d\Omega+\int_{\Omega_L}\gamma_w^2\overline{\mathbf{N}}^T\mathbf{L}\overline{\mathbf{N}}d\Omega$$

and the internal and external force vectors are calculated from

$$\mathbf{f}_a^{ext}=\int_{\Gamma_t}\mathbf{N}^T\mathbf{t}^*d\Gamma\ \ ;\ \ \mathbf{f}_b^{ext}=\int_{\Gamma_t}H_w\mathbf{N}^T\mathbf{t}^*d\Gamma$$
$$\mathbf{f}_a^{int}=\int_{\Omega_N}\mathbf{B}^T\boldsymbol{\sigma}d\Omega+\int_{\Omega_L}\mathbf{B}^T\boldsymbol{\sigma}d\Omega \qquad (43)$$
$$\mathbf{f}_b^{int}=\int_{\Omega_N}H_w\mathbf{B}^T\boldsymbol{\sigma}d\Omega+\int_{\Omega_L}H_w\mathbf{B}^T\boldsymbol{\sigma}d\Omega+\int_{\Omega_L}\gamma_w\overline{\mathbf{N}}^T\boldsymbol{\sigma}d\Omega$$

It can be noticed that, when compared to SDM and WDM, there are more expressions involved for RDM and some of them contain the non-linear terms $H_w, H_w^2, \gamma_w, \gamma_w^2$. These terms imply numerical challenges. It is also noteworthy that the enriching dof's are evaluated at the nodes of the element and the regularized displacement profile in the element is obtained by an interpolation using the regularized tanh-function herein.

4. Discussion

The three methods described in the previous section and whose strain profiles are reported in Fig.5, are now assessed and mutually compared with the aim to identify their pros and cons.

4.1. Regarding the physics

In the post-critical regime, the three methods are *a priori* capable of describing the consequences of ductile damage-induced progressive failure leading to crack formation. In the SDM this is provided by setting up a cohesive law which includes normal and shear components with so far more or less arbitrary evolution laws; whereas in the WDM and RDM it is achieved by adopting a constitutive model which is expected to involve both hydrostatic and deviatoric stresses as well as an additional internal variable kinetics accounting for void coalescence, e.g. [16]. It is noteworthy that in the case of the SDM, it would be also possible to implement a more specific stress triaxiality-dependent cohesive law, see e.g. [17].
Moreover, considering their theoretical framework, the three methods can be extended to model adiabatic shear banding which arises during dynamic loading within a scenario where shear banding precedes micro-voiding, and not the opposite as stated in the present work. This could be achieved in the SDM by keeping in the cohesive law the tangential (shear) component only and in the WDM and RDM by describing a localization band with a finite thickness thus corresponding to the physical appearance of the shear band, see [18].

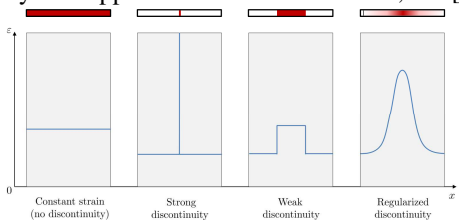

Figure 5: Strain profile for a weak discontinuity.

4.2. Regarding the computational issues

The three localization methods introduce a length scale which serves as localization limiter and thus prevents the post-critical numerical solution from severe mesh (size and orientation) dependence. In the WDM and the RDM, the length scale obviously corresponds to the band width. In the SDM, such a length scale does not appear explicitly in its inherent formulation, see [15] for the SDM, [9] for the WDM and [10] for the RDM.

Concerning the numerical integration, the SDM and WDM may take advantage of a 64-point Gauss rule to integrate the terms related to the bulk material and a 2-point Gauss rule to evaluate the line integrals of either the cohesive segment (SDM) or the band which is numerically reduced to a line (WDM). In the RDM, the numerical integration has turned out to be more difficult as it is important to properly capture the high strain gradient. When the bandwidth is chosen too small with respect to the element size, the regularized discontinuity profile cannot be properly captured by the 64 Gauss point technique. So, specific integration schemes, as discussed in subsection 3.3, have to be applied demanding for cumbersome projection techniques of the path- and history-dependent variables.

4.3. Perspective of a unified approach

Here is discussed the capability of the methods to be incorporated within a unified numerical failure model describing the successive steps leading to the ultimate rupture, viz. (more or less) diffuse damage, strain and damage localization and crack propagation. A proper transition from the pre-localization phase of diffuse damage using standard FEM to the onset of strain localization (marking the start of the post-critical regime) and the straightforward passage from localization to crack propagation have to be ensured. At the onset of

localization, the enriching dof's of the X-FEM are activated in all three methods. In the SDM the initial traction force of the cohesive law in the localized element has to be determined so as to get a smooth transition. In the WDM and RDM there is no need to compute additional values if the same constitutive model is used outside and inside the band. The transition to fracture may be achieved in the three methods as soon as the in-band stresses or tractions vanish and become zero. Then, for the SDM, WDM and RDM it could be shown that the equations for stress-free (standard) X-FEM are naturally obtained.

5. Conclusion

In this paper are presented three embedded-band FE approaches aiming at describing the intermediate stage of strain and damage localization, based on strong discontinuity (SDM), weak discontinuity (WDM) and regularized discontinuity (RDM) methods within X-FEM. The approaches in question are assessed from the physics, computational and unified modelling perspectives. Pros and cons for each approach is outlined in Table 3.The objective is to give some elements for further developments to engineers and researchers working in the field of ductile failure of larges structures. The present work deals with void coalescence induced strain localization. It is noteworthy that strain localization may also result from other structural or/and material instabilities such as e.g. necking [19] or adiabatic shear banding [18].

Table 3: Assets and weak points of the approaches

Strong discontinuity	Weak discontinuity	Regularized discontinuity
⊕ Complex micro-mechanisms collapsed into surface ⊕ Only 1 additional parameter (W_c) ⊕ Reduced mesh dependence (length scale $\frac{W_c}{t_0}$) ⊕ Straightforward integration scheme ⊕ Energy-based failure criterion adapted to ductile materials ⊕ Allows for describing shear banding	⊕ Reduced mesh dependence (length scale $\mathcal{W}$) ⊕ Straightforward integration scheme ⊕ Post-localization behavior accounts for stress triaxiality ⊕ Energy-based failure criterion adapted to ductile materials ⊕ Allows for describing shear banding	⊕ Reduced mesh dependence (length scale $\mathcal{W}$) ⊕ Post-localization behavior accounts for stress triaxiality ⊕ Energy-based failure criterion adapted to ductile materials ⊕ Allows for describing shear banding
⊖ Technique to calculate initial traction t_0 from stress state at localization required	⊖ 2 additional parameters ($\mathcal{W}$,W_c) ⊖ Failure criterion does not satisfy condition of vanishing stress	⊖ 2 additional parameters ($\mathcal{W}$,W_c) ⊖ Failure criterion does not satisfy condition of vanishing stress ⊖ Integration scheme involving variable projection necessary if band width much smaller than element size

References

[1]A. A. Benzerga. Micromechanics of coalescence in ductile fracture. J. Mech. Phys. Sol., 50(6):1331–1362, 2002.

[2]T. Pardoen and J. W. Hutchinson. An extended model for void growth and coalescence. J. Mech. Phys. Sol., 48(12):2467–2512, 2000.

[3]T. Belytschko, J. Fish, and B. E. Engelman. A finite element with embedded localization zones. Comp. Methods Appl. Mech. Eng., 70:59–89, 1988.

[4]M. Ortiz, Leroy Y., and A. Needleman. A finite element method for localized failure analysis. Comp. Methods Appl. Mech. Eng., 61:189–214, 1987.

[5]N. Moës, J. Dolbow, and T. Belytschko. A finite element method for crack growth without remeshing. Int. J. Num. Methods Eng., 46:131–150, 1999.

[6]J. Oliver. Modeling strong discontinuities in solid mechanics via strain softening constitutive equations. part 1: Fundamentals. part 2: Numerical simulation. Int. J. Num. Methods Eng., 39:3575–3624, 1996.

[7]R. A. Regueiro and R. I. Borja. A finite element model of localized deformation in frictional materials taking a strong discontinuity approach. Fin. Elem. An. Des. 33:283-315, 1999

[8]N. Moës and T. Belytschko. Extended finite element method for cohesive crack growth. Eng. Fract. Mech., 69(7):813–833, 2002.

[9]A. E. Huespe, A. Needleman, J. Oliver, and P. J. Sanchez. A finite thickness band method for ductile fracture analysis. Int. J. Plast., 25(12):2349–2365, 2009.

[10]P. Areias and T. Belytschko. Two-scale shear band evolution by local partition of unity. Int. J. Num. Methods Eng., 66(5):878–910, 2006.

[11]E. Benvenuti, A. Tralli, and G. Ventura. A regularized xfem model for the transition from continuous to discontinuous displacements. Int. J. Num. Methods Eng. 74(6):911–944, 2008.

[12]J.-P. Crété, P. Longère, and J.-M. Cadou. Numerical modelling of crack propagation in ductile materials combining the GTN model and X-FEM. Comp. Methods Appl. Mech. Eng., 275:204–233, 2014

[13]M. Jirásek. Comparative study on finite elements with embedded discontinuities. Comp. Methods Appl. Mech. Eng., 188:307–330, 2000.

[14]J. Oliver. Modeling strong discontinuities in solid mechanics via strain softening constitutive equations. part 1: Fundamentals. part 2: Numerical simulation. Int. J. Num. Methods Eng., 39:3575–3624, 1996.

[15]G. N.Wells and L. J. Sluys. A new method for modelling cohesive cracks using finite elements. Int. J. Num. Methods Eng., 50(12):2667–2682, 2001.

[16]J. Wolf, P. Longère, J.-M. Cadou and J.-P. Crété. Numerical modeling of strain localization in engineering ductile materials combining cohesive models and X-FEM. Int. J. Mech. Mater. Design. 14, 177-193. 2018

[17]A. Banerjee and R. Manivasagam. Triaxiality dependent cohesive zone model. Eng. Fract. Mech., 76:1761–1770, 2009.

[18]P. Longère. Adiabatic shear banding assisted dynamic failure: Some modeling issues. Mech. Mater.. 116, 49-66. 2018

[19]S. Mercier, N. Granier, A. Molinari, F. Llorca and F. Buy. Multiple necking during the dynamic expansion of hemispherical metallic shells, from experiments to modelling. J. Mech. Phys. Sol., 58-7:955–982. 2010